DOI: 10.24996/ijs.2023.64.12.11

ISSN: 0067-2904

Synthesis of Green Zno/Fe_3O_4 Nanocomposite by Microplasma Jet and Anti-Bacterial Agent

Sabah N. Mazhir[1*], Neean F. Majeed[1], Ehsan M. Abbas[2], Nisreen kh. Abdalameer[1], Shaymaa A. Qasim[1]

[1]*College of Science for women, University of Baghdad, Baghdad, Iraq*
[2]*Alayen University, Iraq.*

Received: 20/8/2022 Accepted: 11/1/2023 Published: 30/ 12 / 2023

Abstract:

There has been an increase in demand for nanocomposite, which has resulted in large-scale manufacturers employing high-energy processes and harmful solvents. Because of this, the need for environmentally benign "green" synthesis processes has grown. Other methods for making nanocomposite include using plants and plant products, bacteria, fungi, yeast, and algae. Green synthesis has minimal toxicity and is safe for human health and the environment compared to other processes, making it the ideal option for creating nanocomposite materials. This work reveals an environmentally friendly synthesis method for magnetic nanocomposites. In particular, they were using an aqueous extract of Artemisia to obtain ZnO/Fe_3O_4 using cold plasma technology. The magnetic nanocomposite was prepared with different concentrations (0.01, 0.02, and 0.03) of M and (2:8) of the aqueous extract. The structural properties were studied using X-ray diffraction, where the crystal size ranged from 30 to 40 nm, while the surface morphology was studied through the field emission scanning electron microscope, and it was found that the shape of the particles is semi-spherical and within a particle size range of 30 to 60 nm. "Green" magnetic nanocomposites showed low toxicity and high biocompatibility, allowing their application in biomedicine, where magnetic nanocomposites were employed as anti-agents for *E. coli* and *S. aureus* using the agar diffusion method. Its high effect on bacterial inhibition was noted when the concentration was increased, as the diameter of inhibition ranged (11-22) mm for *E. coli* and (15-24) mm for *Staphylococcus aureus.*

Keywords: Green, Artemisia, ZnO: Fe_3O_4, Nano composite, Cold plasma, *E.Coli, S.aureus*

توليف المتراكبات النانوية الخضراء ZnO/Fe_3O_4 باستخدام تقنية نفاث البلازما الدقيقة وتطبيقها كعوامل مضادة للميكروبات

صباح نوري مزهر[1]، نيان فريد مجيد[1]، احسان محسن عباس[2]، نسرين خليل عبدالامير[1]، شيماء علي قاسم[1]

[1]قسم الفيزياء ، كلية العلوم للبنات، جامعة بغداد، العراق
[2]جامعة العين ، ذي قار ، العراق

Email: sabahnm_phys@csw.uobaghdad.edu.iq

الخلاصة:

زيادة الطلب على تحضير المتراكبات النانوية ادى الى تصنيعها بشكل واسع النطاق وباستعمال طاقات عالية ومذيبات ضارة. مما ادى الى ازدياد الحاجة إلى عمليات تحضير "خضراء" صديقة للبيئة، عن طريق إستعمال طرق سهلة وغير مكلفة بمستخلصات نباتية. يحتوي التوليف الأخضر على حد أدنى من السمية، وهو آمن لصحة الإنسان والبيئة مقارنة بالعمليات الأخرى، مما يجعله خيارًا مثاليًا لتخليق المتراكبات النانوية. تكشف هذه الدراسة طريقة توليف المتراكبات النانوية المغناطيسية على وجه الخصوص باستعمال مستخلص مائي لنبات الشيح (Artemisia) للحصول على ZnO / Fe_3O_4 باستعمال تقنية البلازما الباردة. تم تحضير ZnO / Fe_3O_4 المغناطيسية بتراكيز مختلفة (٠.٠٠١و٠.٠٠٢و٠.٠٠٣)مولاري من المستخلص المائي بنسبة (8:2). تمت دراسة الخواص التركيبية باستعمال حيود الأشعة السينية، حيث تراوح الحجم البلوري بين (30–40) نانومتر، بينما تمت دراسة الشكل السطحي من خلال المجهر الإلكتروني الماسح ووجد أن شكل الجسيمات شبه كروية ومتداخلة حيث تراوح حجم الجسيمات (30–60) نانومتر. أظهرت المتراكبات النانوية المغناطيسية "الخضراء" سمية منخفضة وتوافقًا حيويًا عاليًا، مما يسمح بتطبيقها في الطب الحيوي، حيث تم استعمال المتراكبات النانوية المغناطيسية كعوامل مضادة للبكتريا الإشريكية القولونية والعصبية الذهبية باستعمال طريقة الانتشار(اجار)، وقد لوحظ تأثيرها العالي على تثبيط البكتيريا عند زيادة التركيز حيث تراوح قطر التثبيط بين (11–22) ملم للإشريكية القولونية و (15–24) ملم للمكورات العنقودية الذهبية.

1. Introduction

Antibacterial compounds are used in various sectors, including packaging, construction, food, textiles, medicine, and water disinfection. Toxicity, high temperature, and pressure sensitivity are among the organic compounds' drawbacks [1]. A growing number of researchers are focusing on using inorganic metal oxides as a source of antibacterial activity since they are non-toxic, stable in harsh environments, and include mineral components [2]. The antibacterial activities of metal and metal oxide nanoparticles have been extensively documented in the scientific literature [3]. Therefore, due to their unique physical, chemical, and biological features, metal and metal oxide nanoparticles have drawn much interest. The size of these nanomaterials may be adjusted [4]. Tailor-made nanomaterials with the necessary characteristics have also been frequently reported. Developing antibacterial nanoparticles is difficult owing to their stability, cost-effectiveness, and great efficacy [5, 6]. Antibacterial nanomaterials, such as nanoparticles, nanowires, and nanotubes, have a high surface area-to-volume ratio, making them ideal for use in these applications. However, accumulation during preparation is the limiting factor [7, 8].

The dispersion factor of metal oxide nanostructures is important for in vivo and in vitro studies. Among the powdered metal oxides, ZnO is a semiconductor with catalytic, optical, electrical, and significant growth inhibition capabilities [9, 10]. Exposing these semiconductors to UV radiation is necessary to activate them [11]. Because of its high catalytic activity and low toxicity, ZnO is an ideal photocatalytic material among these semiconductors [12]. There are a lot of active sites on ZnO nanoparticles since they have a large surface area. The semiconductor ZnO is an n-type semiconductor. Approximately 3.37 eV [13] is the energy of the broadband gap. ZnO's broadband gap allowed it to be excited in the UV spectrum below 400 nm. Recombination of holes and electrons is another limitation of ZnO [13]. If this problem persists, ZnO may be modified to fix it [14]. This change made it possible to get higher absorption in visible light. The recombination between electrons and holes is also reduced. Many approaches have been developed to circumvent ZnO's limitations, such as doping, surface modification using metal nanoparticles, and heterostructure advancement [14]. For example, the separation rate of electron-hole pairs may be accelerated by coupling ZnO with p-type materials such as Fe3O4 [15]. Consequently, the Fe_3O_4/ZnO nanocomposite's photocatalytic performance is more active because of the holes-to-electrons separation in the p-n junction. Photocatalysts may be isolated and reused from wastewater using an external magnet because of their current magnetic characteristics [16]. To find out how to create nanoparticles, some options include expanding supercritical fluids rapidly, electrospray crystallization, or hot plasmas [17].

All three approaches, however, do not allow for the industrial-scale production of low-cost organic crystals with a nanometer size. While electrospray crystallization may be scaled up, the rapid growth of supercritical solutions is time-consuming and expensive. Nanoparticles may be produced using thermal plasmas, which are both effective and cost-effective [18]. On the other hand, thermal plasmas are not suitable for organic substances due to their high temperature. The breakdown of organic substances is prevented by using cold plasmas, which operate at temperatures near the ambient temperature. The problem is that cold plasmas are generally operated in a vacuum, which makes the process more complex and costly, especially at larger scales [19, 20]. When reasonably high production rates are needed, atmospheric pressure plasma systems are an attractive option for decreasing equipment and processing costs. The dielectric barrier discharge, a cold plasma that may be employed at atmospheric pressure, was used in this work as a particular form of plasma. Synthesis of organic compounds with scalability and low operating costs is possible using atmospheric-pressure cold plasma [21, 22].

2. Experimental setup :

2.1 Synthesis of green ZnO/Fe_3O_4 nanocomposite by cold plasma:

ZnO: Fe3O4 nanoparticles were prepared with molar ratios (0.01, 0.02, and 0.03) M from zinc nitrate $Zn(NO_3)_2.6H_2O$ and iron nitrate $Fe(NO_3)_3.9H_2O$ using artemisia extract. Both zinc and iron nitrate were prepared in the same way, and the following method was used to know the weight per molar:

1. Take (0.3, 0.6, 0.9 gm) for zinc nitrate and (0.24, 0.48, 0.72 gm) for iron nitrate, weighed for each of (0.01, 0.02, 0.03) M.
2. Put in a glass beaker containing 100 ml of distilled water and stir with a magnetic stirrer for 10–15 minutes.
3. Take 5 ml of ZnO and 5 ml of Fe_3O_4 (0.01, 0.02, and 0.03) M, and the compound was placed in a 10 ml small beaker.
4. Exposed to the plasma jet system for 10 minutes to obtain the nanomaterial for each of the three concentrations.

The nanocomposite was prepared using cold plasma technology at a voltage of 15 kV, a frequency of 23 Hz, and a flow rate of 3 l/min of argon gas using Artemisia extract at a ratio of 2:8 at (0.01, 0.02, and 0.03 M) as illustrated in Fig. 1.

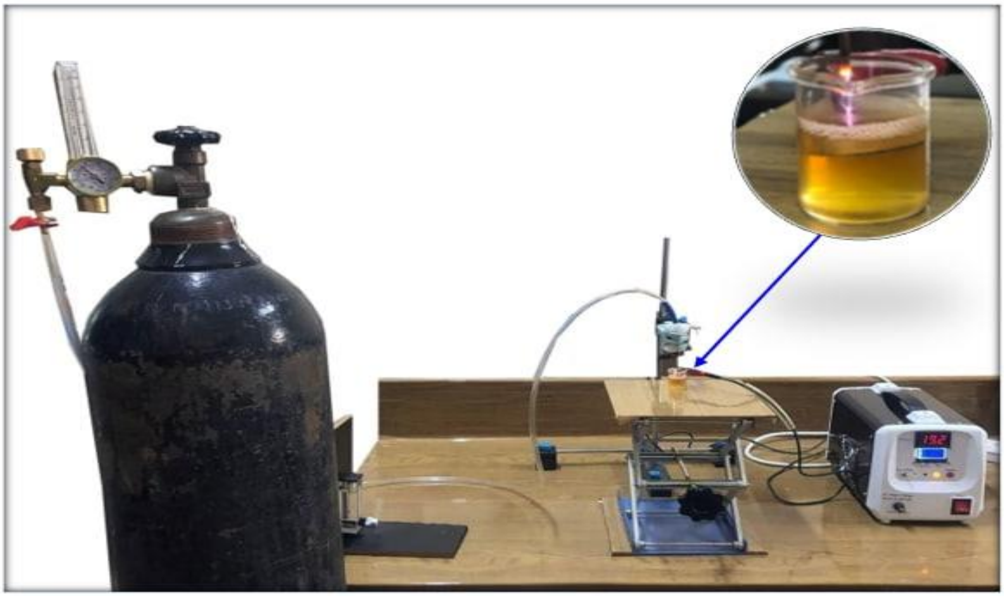

Figure 1: Prepared of Nanocomposite by cold plasma

Study of the effect of Nanocomposite on pathogenic bacteria:

The inhibition activity of the bacteria was tested after choosing the best results on two bacteria types, *Aureus staphylococcus* and *Escherichia coli*, where bacterial isolation and the good diffusion method were used. (Neutrian ager) media and left for 30 minutes at room temperature. After which, a drill is made in the culture medium using a cork drill measuring 6 mm with 3 holes in each plate. And then, we named and marked each hole. This drilling is the prepared solution concentration (0.01, 0.02, and 0.03 M). Without wormwood and with wormwood, 75 microliters of pre-prepared ZnO:Fe_3O_4 particle solution were placed in each hole. The dishes were left at room temperature for a period and then incubated at 37 ^oC for a period of 18–24 hours, after which the inhibition area around the holes was measured in millimeters.

3. Results and Discussion:

3.1 X-ray Diffraction

ZnO: Fe_3O_4+Artemisia Nanoparticles of the crystal structure were examined using the x-ray diffraction spectra obtained with (0.01, 0.02, and 0.03 M) molarity concentrations. The crystal size was estimated using Eq. (1) (Table 1). With the aid of the whole width at half-maximum peak, the average dimension of a crystal, denoted by the symbol D, may be quickly determined from the X-ray range of the full width at half-maximum (FWHM). It can be determined by applying Scherrer's formula [10]. After subtracting the instrumental broadening, the FWHM in radians is the corresponding diffraction angle. The primary peaks of ZnO and Fe3O4 are in Figure 2. Parallel faces in a cubic crystal structure display the X-ray diffraction analysis's findings using examples from the study of ZnO:Fe_3O_4. In Figure 2a, the concentration (0.01)M shows (022), (100), (311), and (102), corresponding to the angles (30.3889^o, 31.8659^o, 36.39^o, and 43.35^o, respectively. In figure 2b, the concentration (0.02)M shows (010), (100), (311), and (311) corresponding to the angles (21.33^o, 31.68^o, and 35.37^o, respectively, and in figure 2c, the concentration (0.03)M reveals the matching values for (022), (100), (311), and (102). It exhibits a high degree of crystallinity, and by increasing the concentration, the crystal size is altered from 34 nm to 41 nm.

$$2d\sin\theta = n\,\lambda \qquad \ldots\ldots (1)$$

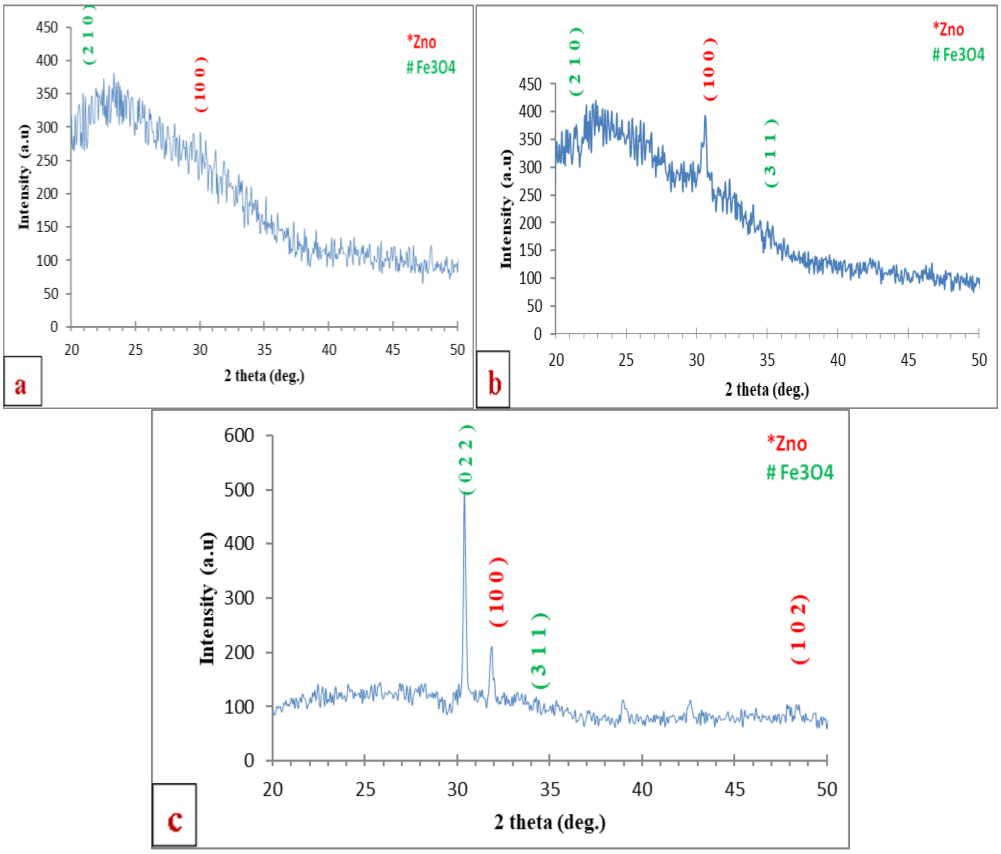

Figure 2: (a, b, and c) X-ray of (ZnO: Fe3O4+ Artemisia) nanocomposite at different concentrations

Table 1: X-ray of ZnO: Fe3O4+ Artemisia Nanocomposite at Different Concentrations

Co. M	2θ (Deg.)	FWHM (Deg.)	C.S (nm)	Av. C.S nm	Phase	hkl	card No.
0.01+Artimisia	**21.7559**	**0.1771**	**45.79539**	**34.54326**	**Fe3O4**	**210**	**96-900-6195**
	31.89	**0.3542**	**23.29114**		**ZnO**	**100**	**96-230-0113**
0.02+Artimisia	**21.33**	**0.1771**	**45.79526**	**38.71136**	**Fe3O4**	**210**	**96-900-6195**
	31.68	**0.1771**	**46.74165**		**ZnO**	**100**	**96-230-0113**
	35.37	**0.3542**	**23.59719**		**Fe3O4**	**311**	**96-900-6195**
0.03+Artimisia	**30.3889**	**0.2952**	**46.61612**	**41.17930**	**Fe3O4**	**220**	**96-900-6195**
	31.8659	**0.3542**	**23.38155**		**ZnO**	**100**	**96-230-0113**
	36.39	**0.1771**	**46.34205**		**ZnO**	**101**	**96-230-0113**
	43.35	**0.1771**	**48.37749**		**Fe3O4**	**400**	**96-900-6195**

3.2 Field emission-scanning electron microscopy (FE-SEM):

The surface morphologies of ZnO: Fe3O4 +Artimisia with different concentrations in particular have been investigated using Field Emission Scanning Electron Microscopy (FE-SEM). As shown in Fig. 3, the FE-SEM image indicates that the ZnO: Fe3O4 +Artimisia nanoparticles had a diameter of approximately 10–100 nm, which proves the nanosize of the prepared samples with different concentrations (0.01, 0.02, 0.03) M.

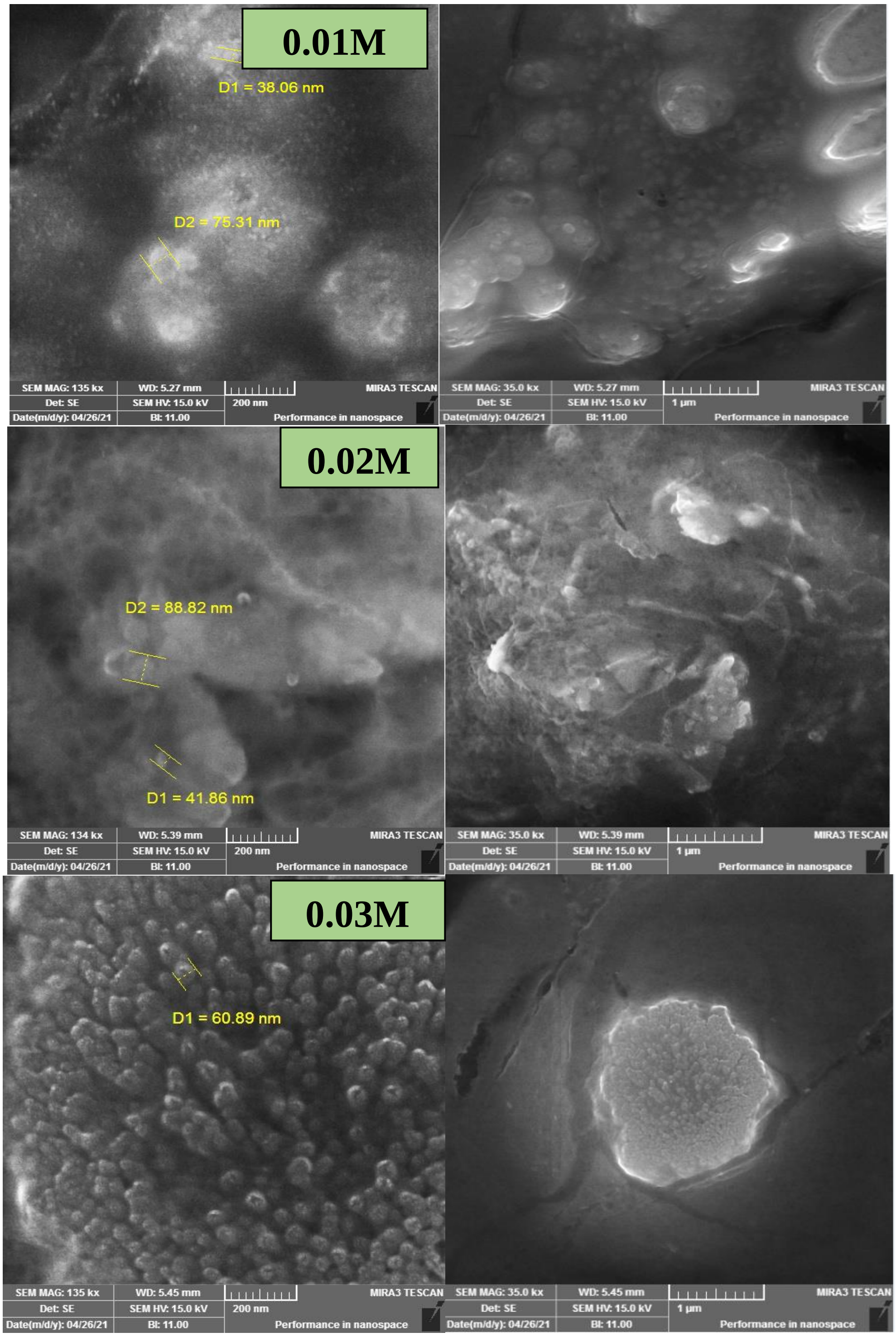

Figure 3: FE-SEM images for (ZnO: Fe3O4+Artemisia) nanocomposite at different concentrations (0.01, 0.02, 0.03) M

3.3 Optical properties

In semiconductor physics, the optical energy gap is one of the most often used expressions in the essential constants of light scattering and refraction. How useful semiconductors are for optical and electrical applications depends on the value of this constant. Figure 4 displays the final spectrum achieved on ZnO: Fe_3O_4+ Artemisia. All the spectrum information that has been gathered revealed a substantial cut-off at wavelengths 420, 433, and 435 nm, where the absorbance value is lowest. Assuming a direct energy gap value for the ZnO: Fe_3O_4+ Artemisia nanocomposite at various concentrations of (0.01, 0.02, and 0.03) M, it is determined in Fig. 4. It can be seen that when concentrations grow, the EG will close, resulting in a reduction in particle size. This is consistent with XRD studies showing that grain size reduces as concentrations rise. To calculate the energy gap, researchers looked at how absorption changed as one moved closer to the basic absorption in the spectrum. Eq. (2) [18] is employed in Table 2.

$$E_g = hc / \lambda \qquad \text{...... (2)}$$

With the rise in concentrations, energy gap values were reduced. The number of photon collisions with the substance increased with concentration, which explains the observed drop. As a result, the material will absorb more photons, and the energy gap will narrow. This narrowing of the energy gap will cause the distribution of atoms within the material to be regulated and the crystal phases to change.

By decreasing the energy gap, the grain size will shrink. Large particle size (at higher concentrations) might result in additional energy states and a diminished confinement effect, which generates a small bandgap, explaining why this is happening.

Table 2: The values of E_g of (ZnO: Fe_3O_4 +Artemisia)

Concentrations (M)	λ= Cut off wavelength (nm)	Eg(eV)
0.01	417	**2.97**
0.02	430	**2.88**
0.03	440	**2.81**

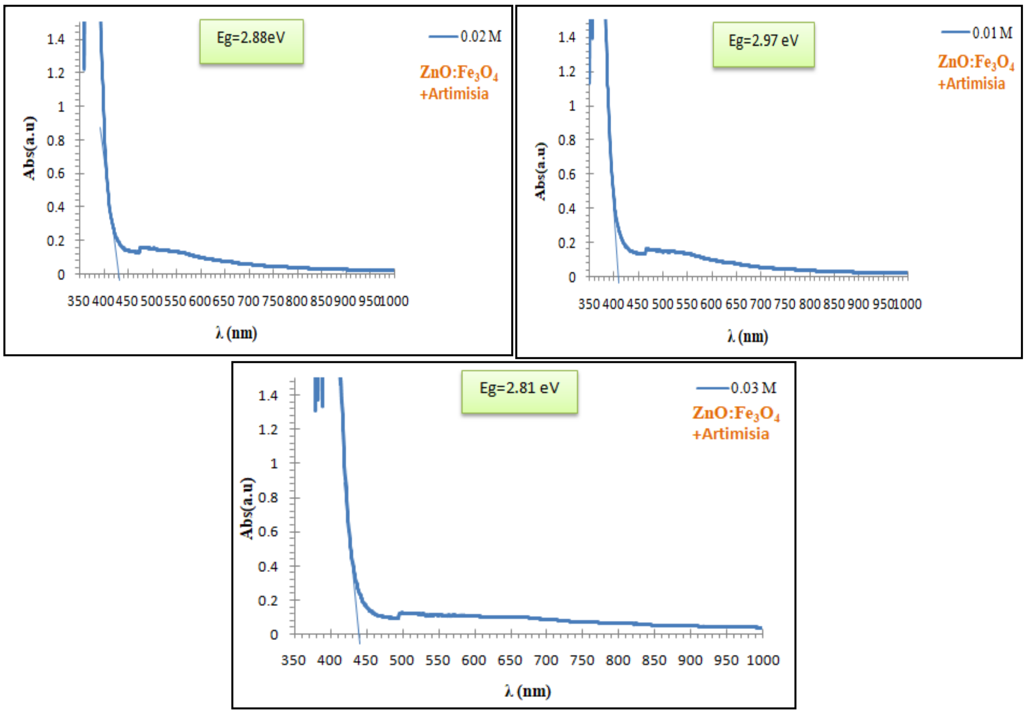

Figure 4: E_g for (ZnO: Fe_3O_4+Artemisia) at different concentrations

3.4 Inhibiting activity of bacteria:

This study tested the antibacterial efficacy of a synthesized (ZnO:Fe3O4) nanocomposite to resist two strains of E. coli and Staphylococcus aureus. Nanoparticles of ZnO:Fe_3O_4 prepared by treating Artemisia leaf extract with ZnO:Fe3O4 nitrate were found to be antibacterial against

Gram-positive and Gram-negative bacteria when evaluated by the agar diffusion method. This study shows that nanoparticles made from plant extract successfully prevent the development of bacterial strains or isolates employed, with the findings of research on inhibitory activity varying with bacterial type and concentration demonstrating the usefulness of nanoparticles. $ZnO:Fe_3O_4$ nanoparticles, on the other hand, were very successful at inhibiting bacteria of both gram-positive and gram-negative varieties.

Also in Fig. 5, observed were $ZnO:Fe_3O_4$ nanoparticles made from Artemisia extract (green method). Inhibiting bacterium activity was observed to decrease in both positive and negative ways. This indicates that the herb made $ZnO:Fe_3O_4$ nanoparticles less toxic. In addition, the function of the bacterium Staphylococcus aureus in blocking it was demonstrated. Table 3 illustrates the findings of ZnO: Fe_3O_4-induced bacterial inhibition particles were made with a 1 ml molar concentration of zinc and iron nitrate and a 2:8 mixing ratio, where the $ZnO:Fe_3O_4$ proportion is 8 and the Artemisia extract percentage is 2. The inhibitory zone diameter was 11 mm at a concentration of 0.01 M in a solution of $ZnO:Fe_3O_4$ nanoparticles made with Artemisia extract. At a concentration of 0.02 M, the diameter of the zone was 15 mm, and at a concentration of 0.03 M, it was 20 mm (22 mm). Previously, table 2 showed that at concentrations of 0.01M and 0.02M, coli-form bacteria were inhibited to the same degree (15 and 17 mm, respectively), whereas at concentrations of 0.03M and 0.04M, the most significant suppression was achieved (25 mm and 30 mm, respectively) (24 mm).

Because bacteria have negative charges and nanometallic oxides have positive charges, there is an electrical attraction between the surface of the bacteria and the nanoparticles. Additionally, nanoparticles produce ions that interact with the group of carrier proteins. Nutrients leak out of the membrane of a bacterial cell and cause the membrane's permeability to decrease, killing the cell [23]. Since it blocks nanoparticles from entering the cell wall, this multilayer is thicker and more solid than peptidoglycan. The cell walls of gram-negative and gram-positive bacteria are structurally distinct because of different lipopolysaccharides and lipoproteins in the former and higher lipid content in the latter, respectively [24]. It was found from the above that the inhibition activity of *E.coli* was higher in all conditions than that of *staph*. bacteria.

Table 3: Inhibition zone of *S.aureus and E.coli* bacteria *at 0.01, 0.02, and 0.03 M* for ZnO: Fe_3O_4+Artemizinin

Concentration%	Types of bacteria	Inhibition zone with Artemisia mm
0.01	**S. aureus**	**11**
0.02		**15**
0.03		**22**
0.01	**E.coli**	**15**
0.02		**17**
0.03		**24**

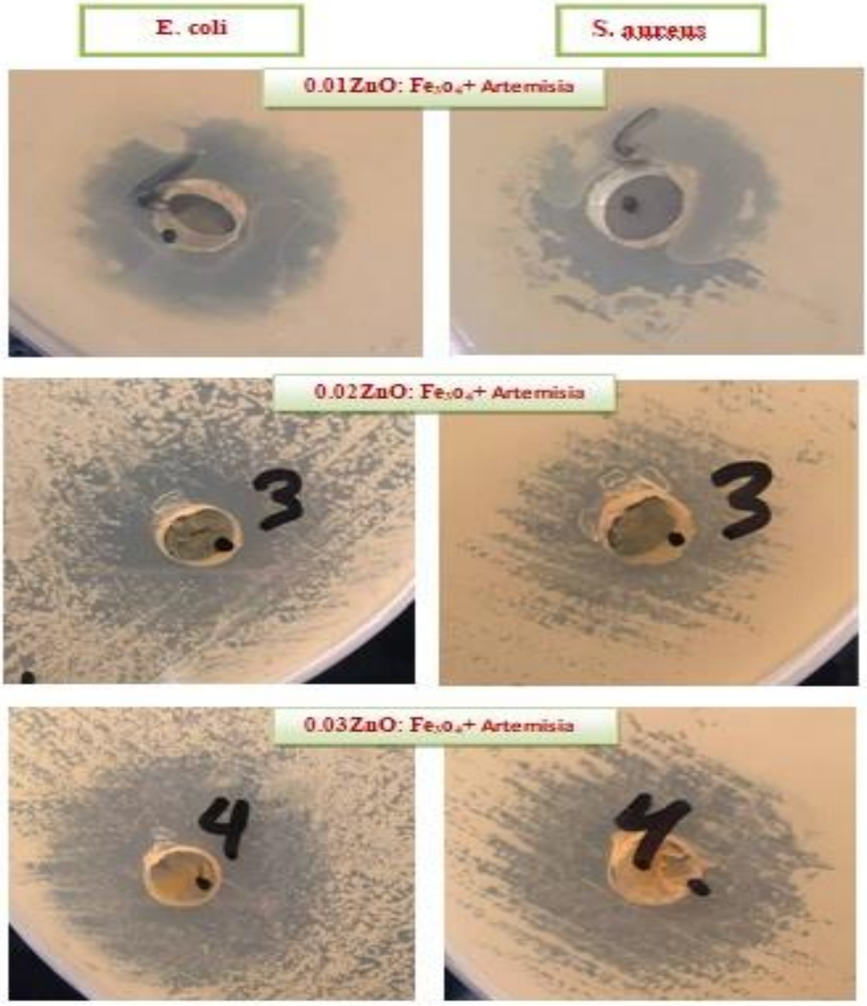

Figure 5: Inhibition zone of Staph bacteria and E.coli bacteria at different concentrations of ZnO: Fe_3O_4+Artemisia

5. Conclusion:

The synthesis of green ZnO/Fe3O4 nanocomposites was achieved by microplasma jet technology. The nanocomposites were characterized by field emission scanning electron microscopy and XRD techniques, where the crystal size ranged from 30 to 40 nm. The surface morphology was studied through the field emission scanning electron microscope, and it was found that the shape of the particles is semi-spherical and within a particle size range of 30–60 nm. Antimicrobial studies have further evaluated the developed nanocomposites. The nanocomposites showed more efficacy for *S. aureus* than for the second type of *E. coli* due to the thickness of the bacteria's cell membrane.

References

[1] Q. Li, S. Mahendra, D. Y. Lyon, L. Brunet, M. V. Liga, D. Li, P. J. Alvarez, "Antimicrobial nanomaterials for water disinfection and microbial control: Potential applications and implications," *Water Res*, vol. 42, pp. 4591–4602, 2008. http://dx.doi.org/10.1016 /j.watres. 2008.08.015.

[2] O. Yamamoto, "Influence of particle size on the antibacterial activity of zinc oxide," *Int. J. Inorganic Mater.*, vol. 3, pp. 643–646, 2001.http://dx.doi.org/10.1016/S1466-6049(01)00197-0.

[3] L. Zhang, Y. Jiang, Y. Ding, M. Povey, D. York, "Investigation into the antibacterial behavior of suspensions of ZnO nanoparticles (ZnO nanofluids)," *J. Nanopart. Res.*, vol. 9, pp. 479–489, 2007.http://dx.doi.org/10.1007/s11051-006-9150-1.

[4] J. Siregar, K. Sebayang, B. Yuliarto, S. Humaidi, "XRD characterization of Fe_3O_4-ZnO nanocomposite material by the hydrothermal method," In: *AIP Conference Proceedings. AIP Publishing LLC*, 2020; 2221: 110008.https://doi.org/10.1063/5.0003210.

[5] R. Brayner, R. Ferrari-Iliou, N. Brivois, S. Djediat, M. F. Benedetti, F. Fiévet, "Toxicological impact studies based on escherichia coli bacteria in ultrafine Zno nanoparticles colloidal medium," *Nano Lett.*, vol. 6, pp. 866–870, 2006.http://dx.doi.org/10.1021/nl052326h.

[6] I. A. Z. Al-Ogaidi, "Camellia sinensis (Green Tea) Mediated Synthesis of Zinc Oxide Nanoparticles and Detect its Antibacterial Activity against Escherichia coli, Staphylococcus aureus and Acinetobacter baumannii," *Journal of Biotechnology Research Center*, vol. 11, no.1, pp. 34-40, 2017.

[7] N. K. Abdalameer, S. N. Mazhir, H. M. Salim, J. K. Hammood, Z. A. Raheem, "Design of micro-jet plasma system: a novel nanoparticles manufacturing method in atmospheric pressure," *Journal of Optoelectronic and Biomedical Materials*, vol. 14, no. 4, pp. 203-210, 2022.

[8] K. A. Thejeel, S. A. Alsahib, I. F. Ascar, M. A. Hussein, "Synthesis of new polymers linked to heterocyclic using zinc oxide with nano structures extracted from natural sources," *Egypt. J. Chem.*, vol. 65, no. 4, pp. 579–589, 2022.

[9] R. Scaffaro, L. Botta, A. Maio, G. Gallo, "PLA Graphene nanoplatelets nanocomposites: Physical properties and release kinetics of an antimicrobial agent," *Composites*, vol. 109, No. Part B, pp. 138–146, 2017.http://dx.doi.org/10.1016/j.compositesb.2016.10.058.

[10] N. K. Abdalameer, L. A. Yaaqoob, J. K. Hammood, "Bio-Synthesis of (Zn/Se) Core-Shell Nanoparticles by Micro Plasma-Jet Technique," *International Journal of Nanoscience*, vol. 21, no. 5, p. 2250041-914, 2022.

[11] C. Linand K. S. Lin, "Photocatalytic oxidation of toxic organohalides with TiO_2/UV: The effects of humic substances and organic mixtures," *Chemosphere*, vol. 66, no. 10, pp. 872-1877, 2007.

[12] R. Abo, N. A. Kummer, B.J. Merkel, "Optimized photodegradation of Bisphenol A in water using ZnO, TiO_2 and SnO_2 photocatalysts under UV radiation as a decontamination procedure," *Drinking Water Engineering and Science*, vol. 9, no. 2, p. 27, 2016.

[13] J. Yu, X. Yu, "Hydrothermal synthesis and photocatalytic activity of zinc oxide hollow spheres," *Environmental Science & Technology*, vol. 42, no. 13, pp. 4902-4907, 2008.

[14] E. A. Martín-Tovar, R. Castro-Rodríguez, "Iribarren A. Isoelectronic CdTe-doped ZnO thin films grown by PLD," *Mater Lett.*, vol. 139, pp. 352–354, 2015.

[15] H. N. Ulya, A. Taufiq. "Comparative structural properties of nanosized ZnO composites prepared by sonochemical and Sol-Gel methods," In: *IOP Conference Series: Earth and Environmental Science. IOP Publishing;* vol. 276, p. 12059, 2019.

[16] A. Akhundi,A. Habibi-Yangjeh, "Ternary magnetic g-C3N4/Fe_3O_4/AgI nanocomposites: novel recyclable photocatalysts with enhanced activity in degradation of different pollutants under visible light," *Materials Chemistry and Physics*, vol. 174, pp. 59-69. 2016.

[17] N. F. Majeed, M. R. Naeemah, A. H. Ali, "Spectroscopic analysis of clove plasma parameters using optical emission spectroscopy," *Iraqi Journal of Science*, vol. 62, no. 8, pp. 2565–2570, 2021.

[18] S. N. Mazhir, N. A. Abdullah, A. F. Rauuf, A. H. Ali, H. I. al-Ahmed, "Effects of Gas Flow on Spectral Properties of Plasma Jet Induced by Microwave," *Baghdad Science Journal*, vol.15, no.1, p. 0081, 2018. https://doi.org/10.21123/bsj.2018.15.1.0081.

[19] R. Matthes, O. Assadian, A. Kramer, "Repeated applications of cold atmospheric pressure plasma does not induce resistance in Staphylococcus aureus embedded in biofilms," *GMS Hyg. Infect. Control*, vol. 9, no. 3, 2014. Doi: 10.3205/dgkh000237.

[20] A. H. Ali, Z. H. Shakir, A. Mezhir, "Influence of Cold Plasma on Sesame Paste and the Nano Sesame Paste Based on Co-occurrence Matri," *Baghdad Science Journal*, vol. 19, no. 4, pp. 855-864, 2022. http://dx.doi.org/10.21123/bsj.2022.19.4.0855.

[21] L. Lin, S. Starostin, Li S, V. Hessel, "Synthesis of metallic nanoparticles by microplasma," *Phys. Sci. Rev.*,vol. 3, no. 1, 2019. Doi: 10.1515/psr-2017-0121.

[22] A. A. Hussain,A. Al-Razzaq, "Plasma characteristics of Ag: Al alloy produced by fundamental and second harmonic frequencies of Nd: YAG laser," *Iraqi J Phys.*, vol. 14, no. 31, pp. 205–214, 2016.

[23] F. Ahmadi, A. H. Kordestany, “Investigation on silver retention in different organs and oxidative stress enzymes in male broiler fed diet supplemented with powder of nano silver,” *Am J Toxicol Sci.*, vol. 3, no. 1, pp. 28–35, 2011.
[24] B. Ivănescu, A. F. Burlec, F. Crivoi, C. Roșu, and A. Corciovă, "Secondary Metabolites from Artemisia Genus as Biopesticides and Innovative Nano-Based Application Strategies," *Molecules*, vol. 26, no. 10, pp. 3061, 2021.